

1 **Spectrum of slip behavior in Tohoku fault zone samples at plate tectonic**  
2 **slip rates**

3 Matt J. Ikari<sup>1\*</sup>, Yoshihiro Ito<sup>2</sup>, Kohtaro Ujiie<sup>3</sup>, Achim J. Kopf<sup>1</sup>

4 <sup>1</sup>MARUM, Center for Marine Environmental Sciences, University of Bremen, Germany

5 <sup>2</sup>Disaster Prevention Research Institute, Kyoto University, Japan

6 <sup>3</sup>Graduate School of Life and Environmental Sciences, University of Tsukuba, Japan

7 \*corresponding author ([mikari@marum.de](mailto:mikari@marum.de))

8

9 **During the 2011 Tohoku-oki earthquake, extremely extensive coseismic slip**  
10 **ruptured shallow parts of the Japan Trench subduction zone and breached the**  
11 **seafloor<sup>6,7</sup>. This part of the subduction zone also hosts slow-slip events<sup>8,9</sup>. The fault**  
12 **thus seems to have a propensity for slip instability or quasi-instability that is**  
13 **unexpected on the shallow portions of important fault zones. Here we use laboratory**  
14 **experiments to slowly shear samples of rock recovered from the Tohoku-oki**  
15 **earthquake fault zone as part of the Japan Trench Fast Drilling project. We find**  
16 **that infrequent perturbations in rock strength appear spontaneously as long-term**  
17 **slow-slip events when the samples are sheared at a constant rate of about 8.5 cm/yr,**  
18 **equivalent to the plate convergence rate. The shear strength of the rock drops by 50**  
19 **to 120 kPa, which is 3 to 6%, over about 2 to 4 hours. Slip during these events**  
20 **reaches peak velocities of up to 25 cm/yr, similar to slow-slip events observed in**  
21 **several circum-Pacific subduction zones. Furthermore, the sheared samples exhibit**  
22 **the full spectrum of fault-slip behaviors, from fast unstable slip to slow steady creep,**  
23 **which can explain the wide range of slip styles observed in the Japan Trench. We**

24 **suggest that the occurrence of slow-slip events at shallow depths may help identify**  
25 **fault segments that are frictionally unstable and susceptible to large coseismic slip**  
26 **propagation.**

27         At the Japan Trench subduction zone, microseismicity observations from ocean  
28 bottom seismometers<sup>1</sup>, distribution of aftershock hypocentral depths<sup>2,3</sup>, and GPS  
29 measurements of slip deficit<sup>4</sup> all indicate that the Japan Trench exhibits an “aseismic”  
30 zone free of earthquake nucleation at depths shallower than 10 km. This is consistent  
31 with the previous conceptual model where the shallowest reaches of subduction  
32 megathrusts were considered to be outside the “seismogenic zone” and thus were  
33 expected to slip aseismically<sup>5</sup>. However, this view must be revised after the 2011  $M_w =$   
34 9.0 Tohoku-Oki earthquake at the Japan Trench generated an estimated 50-80 m of  
35 coseismic, tsunamigenic slip reaching the seafloor based on geodetic data and repeated  
36 bathymetry surveys<sup>6,7</sup>. In addition, the Japan Trench has a long record of slow and  
37 tsunamigenic earthquakes at shallow depths in this region<sup>8,9</sup>, which is not considered  
38 typical of an aseismic, creeping fault zone. Recent evidence thus demonstrates that the  
39 near-trench portions of plate-boundary faults can fail in a wide range of slip styles, and an  
40 important unresolved question is therefore whether laboratory-measured frictional  
41 properties can explain and be used to simulate slip behavior on the shallow Japan Trench  
42 megathrust.

43         Predicting the slip style of faults relies heavily on laboratory friction experiments,  
44 which have shown that aseismic slip is favored in materials that strengthen with increased  
45 slip velocities (velocity-strengthening friction)<sup>5</sup>. This type of behavior is prevalent in  
46 unconsolidated, weak clay-rich sediments<sup>10</sup>, which are common in the shallow portions

47 of subduction thrusts<sup>11</sup>. One possible exception is sediment with a high smectite content,  
48 which is known to be extremely weak but also exhibits some instances of velocity-  
49 weakening friction<sup>12</sup>, which is necessary for slip instability. Specifically, velocity  
50 weakening in smectite has been observed at low normal stress (< 30 MPa), intermediate  
51 sliding velocity (0.2 to 30  $\mu\text{m/s}$ ), and room temperature ( $\sim 20^\circ\text{C}$ ), but under room  
52 humidity and not fluid saturated. The origin of velocity weakening in smectite is not  
53 well understood.

54         During Integrated Ocean Drilling Program Expedition 343, the Japan Trench Fast  
55 Drilling Project (JFAST), samples of the plate boundary fault zone were recovered  $\sim 7$  km  
56 landward of the Japan Trench axis at 822 meters below seafloor (mbsf), within the region  
57 of largest coseismic slip during the 2011 Tohoku earthquake<sup>13</sup> (Figure 1). Mineralogic  
58 analyses of the highly deformed, foliated fault zone indicate smectite content of  $\sim 80\%$  in  
59 the bulk sediment<sup>14</sup>. As expected from previous work on smectite, friction experiments  
60 within the range 0.1-30  $\mu\text{m/s}$  indicate that the fault zone is both weak and velocity  
61 strengthening but with a few cases of velocity weakening<sup>15</sup>, and at coseismic slip  
62 velocities of  $\sim 1$  m/s exhibits very low friction coefficients<sup>16</sup> ( $\mu < 0.2$ ). This seems to  
63 indicate potential for slip instability, however pre-earthquake faults are initially moving  
64 at plate convergent rates (or slower in cases of full or partial locking), orders of  
65 magnitude slower than typical laboratory rates. We investigate here the frictional  
66 behavior of the shallow Tohoku megathrust, using slow laboratory experiments  
67 conducted at the convergence rate between the Pacific and North American plates of 8.5  
68 cm/yr, or 2.7 nm/s (ref 17) in order to accurately simulate an interseismic megathrust  
69 fault zone.

70 We deform four cylindrical samples (25 mm height, 25 mm diameter): two intact  
71 and two powdered core samples from the plate boundary fault zone in a single-direct  
72 shear configuration<sup>15</sup> to measure the coefficient of sliding friction  $\mu = \tau/\sigma_n'$ , where  $\tau$  is  
73 the shear strength and  $\sigma_n'$  is the effective normal stress, and friction velocity dependence  
74  $a-b = \Delta\mu/\Delta\ln v$ , where  $v$  is the sliding velocity<sup>5</sup>. To approximate in-situ conditions near  
75 the trench (assuming hydrostatic pore pressure) samples were sheared at  $\sigma_n' = 7$  MPa  
76 with 3.5% NaCl brine as pore fluid; samples are allowed fully consolidate prior to  
77 shearing so that the pore pressure is assumed negligible. In our tests, we sheared the  
78 samples at 10  $\mu\text{m/s}$  for  $\sim 5$  mm to establish steady-state shear geometry and residual  
79 friction level, then subsequently decreased the slip velocity to the plate rate value of 2.7  
80 nm/s, simulating realistically slow initial fault slip rates.

81 At 10  $\mu\text{m/s}$  we observe a distinct peak in friction of  $\mu = 0.23-0.30$  for both  
82 powdered and intact samples, that decreases to residual values of  $\sim 0.22$  for intact and  
83  $\sim 0.16$  for powdered samples (Figure 2). High-frequency (recurrence  $\sim 0.5$  s), low-  
84 amplitude (10-20 kPa,  $\sim 1-2\%$  stress drop) stick-slip behavior is observed upon attainment  
85 of residual friction levels. After the decrease in velocity to the plate rate, friction  
86 increases to 0.21-0.24 for both intact and powdered samples. Clear stick-slip behavior  
87 was initially observed which ceased as friction evolved to a new residual level; stress  
88 drops for these events are similar to those at 10  $\mu\text{m/s}$  ( $\sim 10$  kPa,  $\sim 1\%$ ) but have a much  
89 longer recurrence ( $\sim 20$  min). The duration of the stick-slip events at both 10  $\mu\text{m/s}$  and  
90 2.7 nm/s is smaller than 0.3 s, our smallest recording interval. Values of  $a-b$  calculated  
91 from the drop from 10  $\mu\text{m/s}$  to 2.7 nm/s range from -0.009 to -0.002; results of 3-fold  
92 velocity steps indicate  $a-b = -0.006$  to -0.003. This is significantly more velocity

93 weakening than the  $a$ - $b$  values of -0.001 to 0.003 measured on the same samples at higher  
94 rates of 0.1-30  $\mu\text{m/s}$  (ref 15). The observations of velocity-weakening friction and stick-  
95 slip behavior clearly demonstrate the propensity for unstable frictional slip, indicating  
96 that the shallow megathrust at the Japan Trench is capable of hosting earthquake  
97 nucleation in addition to facilitating rupture propagation.

98         When steady-state strength is re-established following the decrease to the plate  
99 rate, shearing proceeds mostly as stable creep. However, larger infrequent strength  
100 perturbations spontaneously occur two to three times over several mm (Figure 2), these  
101 occur most frequently in tests using intact samples, and were not observed in a control  
102 experiment in which powdered Rochester shale was tested as an illite-rich, velocity-  
103 strengthening reference material<sup>12</sup>. We observe stress increases before the stress drop so  
104 that the friction level before and after the event are similar. Records of shear  
105 displacement which have been detrended for the target slip velocity show clear deviations  
106 during these events, with a slip deficit occurring during the loading phase and a slip  
107 excess occurring during the stress drop. The stress drop for these events ranges from 50-  
108 120 kPa, which represents 3-6% of the shear strength. The stress drop occurs over 2-4  
109 hours, with maximum slip rates during these events ranging from 3-8 nm/s (10-25  
110 cm/year).

111         The larger, irregular events we observe are distinctly different from ordinary  
112 stick-slip behavior or slower oscillatory slip<sup>18</sup>. Based on the duration of the stress drop  
113 and magnitude of the slip velocity, we interpret these events to be laboratory-generated  
114 slow slip events (SSE). These slow events hold several similarities to numerically  
115 simulated spontaneous periodic or aperiodic slip transients, including the slip rate, low

116 effective stresses, and conditional stability suggesting that some amount of velocity-  
117 weakening friction is necessary<sup>19</sup>. Our observation that stick-slip at the plate rate is only  
118 observed during a transient phase of increasing friction following a velocity decrease, and  
119 subsequently gives way to a combination of creep and SSE, suggests that the frictional  
120 stability of the system evolves toward conditional stability. Considering constant  
121 (effective) normal stress, apparatus stiffness, and consistent velocity-weakening we  
122 speculate that this evolution may be related to a critical slip distance for dynamic  
123 weakening<sup>5</sup>. Because we observe SSE most often in our intact samples, the frictional  
124 properties conducive for SSEs may be associated with scaly fabric developed in-situ.

125         Slow earthquakes and transient slip events observed in natural tectonic settings  
126 can vary widely in terms of duration, total slip, and equivalent seismic moment<sup>20</sup>.  
127 However, we find that the (maximum) slip velocities we observe, 10-25 cm/yr, are  
128 strikingly similar to those of silent earthquakes or SSE observed in several subduction  
129 zones<sup>22-30</sup> (Figure 3). Calculated equivalent moment magnitudes of these SSEs range  
130 from  $M_w = 6.6-7.5$ . A notable feature of most observed natural SSE is that they occur at  
131 the lower seismogenic zone boundary or immediately downdip. Our samples were  
132 recovered from < 1 km depth at the Japan Trench, consistent with SSEs that occur above  
133 or near the shallower updip limit of the seismogenic zone. Shallower SSEs are observed  
134 less frequently, but this is likely due to sparser offshore instrumentation and may be more  
135 a more common phenomenon. Inversion of GPS data at the northern Costa Rica margin  
136 near Nicoya Peninsula reveal two SSEs; one is located at the downdip seismogenic zone  
137 boundary at 25-30 km, but another slip patch is observed at ~6 km depth near the updip  
138 limit<sup>30</sup>. Ito et al. (2013) observed two SSEs prior to the 2011 Tohoku earthquake; one in

139 November 2008 ( $M_w = 6.8$ ) and one in February 2011 ( $M_w = 7.0$ ) that was likely still  
140 ongoing at the time of the earthquake. Slip velocities are estimated to be 360 cm/yr,  
141 much faster than the velocities of our laboratory SSE. However, the estimated stress  
142 drops of the Tohoku SSE are 50-100 kPa, which match our observed stress drops of 50-  
143 120 kPa. Dislocation modeling indicates that these SSE occurred at 10-15 km depth,  
144 within the seismogenic zone and co-located with the rupture area of the Tohoku  
145 earthquake. We therefore suggest that despite some spatial variations, the entire shallow  
146 plate boundary from ~15 km depth to the trench is capable of generating SSEs with an  
147 equivalent  $M_w$  of ~7.

148 In addition to producing the SSEs observed prior to the 2011 Tohoku earthquake,  
149 the frictional properties of the fault zone likely contributed to large near-trench coseismic  
150 slip during the earthquake, either due to active weakening during an SSE<sup>9</sup> or by  
151 inherently unstable slip. Most notably this includes evidence of frictional instability (by  
152 stick-slip) or capacity for instability (by velocity weakening), but our results also  
153 demonstrate that the Tohoku fault zone exhibits the full spectrum of slip behaviors. One  
154 important implication is that in the absence of significant seismicity, the occurrence of  
155 SSEs on the shallow portions of major faults may be diagnostic of potential slip  
156 instability and near-surface coseismic slip in other subduction zones.

157

## 158 **Acknowledgements**

159 This research uses samples and/or data provided by the Integrated Ocean Drilling  
160 Program (IODP). We are thankful for discussions with the IODP Expedition 343  
161 scientific party, and Heather Savage and an anonymous reviewer for their constructive

162 comments. This work was supported by the Deutsche Forschungsgemeinschaft (DFG)  
163 Grant #IK107/1-1 to M.I.

164

#### 165 **Author contributions**

166 M.I. conducted friction experiments and data analysis. All authors contributed to  
167 planning and writing the manuscript.

168

#### 169 **References**

- 170 1. Nishizawa, A., Kanazawa, T., Iwasaki, T. & Shimamura, H. Spatial distribution  
171 of earthquakes associated with the Pacific plate subduction off northeastern Japan  
172 revealed by ocean bottom and land observation. *Phys. Earth Planet. Int.* **75**, 168-  
173 175 (1992).
- 174 2. Hino, R. et al. Aftershock distribution of the 1994 Sanriku-oki earthquake ( $M_w$   
175 7.7) revealed by ocean bottom seismographic observation. *J. Geophys. Res.* **105**,  
176 21,697-21,710 (2000).
- 177 3. Obana, K. et al. Aftershocks near the updip end of the 2011 Tohoku-Oki  
178 earthquake. *Earth Planet. Sci. Lett.* **382**, 111-116 (2013).
- 179 4. Hashimoto, C., Noda, A., Sagiya, T. & Matsu'ura, M. Interplate seismogenic  
180 zones along the Kuril-Japan trench inferred from GPS data inversion. *Nat. Geosci.*  
181 **2**, 141-144 (2009).
- 182 5. Scholz, C.H. Earthquakes and friction laws. *Nature* **391**, 37-42 (1998).
- 183 6. Fujiwara, T. et al. The 2011 Tohoku-Oki earthquake: Displacement reaching the  
184 trench axis. *Science* **334**, 1240 (2011).



- 185 7. Ito, Y. et al. Frontal wedge deformation near the source region of the 2011  
186 Tohoku-Oki earthquake. *Geophys. Res. Lett.* **38**, L00G05 (2011).
- 187 8. Fukao, Y. & Kanjo, K. A zone of low-frequency earthquakes beneath the inner  
188 wall of the Japan Trench. *Tectonophys.* **67**, 153-162 (1980).
- 189 9. Ito, Y. et al. Episodic slow slip events in the Japan subduction zone before the  
190 2011 Tohoku-Oki earthquake. *Tectonophys.* **600**, 14-26 (2013).
- 191 10. Ikari, M.J., Saffer, D.M. & Marone, C. Frictional and hydrologic properties of  
192 clay-rich fault gouge. *J. Geophys. Res.* **114**, B05409 (2009).
- 193 11. Underwood, M.B. in *The Seismogenic Zone of Subduction Thrust Faults* (eds.  
194 Dixon, T.H. & Moore, J.C.) 42-84 (2007)
- 195 12. Saffer, D.M., & Marone, C. Comparison of smectite- and illite-rich gouge  
196 frictional properties: application to the updip limit of the seismogenic zone along  
197 subduction megathrusts. *Earth Planet. Sci. Lett.* **215**, 219-235 (2003).
- 198 13. Chester, F.M., Mori, J.J., Eguchi, N., Toczko, S. & Expedition 343/343T  
199 Scientists. *Proc. IODP*, **343/343T**: Integrated Ocean Drilling Program  
200 Management International, Inc., Tokyo (2013).
- 201 14. Kameda, J. et al. Pelagic smectite as an important factor in tsunamigenic slip  
202 along the Japan Trench. *Geology* (2015).
- 203 15. Ikari, M.J., Kameda, J., Saffer, D.M. & Kopf, A.J. Strength characteristics of  
204 Japan Trench borehole samples in the high-slip region of the 2011 Tohoku-Oki  
205 earthquake. *Earth Planet. Sci. Lett.* **412**, 35-41 (2015).
- 206 16. Ujiie, K. et al. Low coseismic shear stress on the Tohoku-Oki megathrust  
207 determined from laboratory experiments. *Science* **342**, 1211-1214 (2013).

- 208 17. DeMets, C., Gordon, R.G., Argus, D.F. & Stein, S. Effect of recent revisions to  
209 the geomagnetic reversal time scale on estimates of current plate motions.  
210 *Geophys. Res. Lett.* **21**, 2191-2194 (1994).
- 211 18. Baumberger, T., Berthoud, P. & Caroli, C. Physical analysis of state- and rate-  
212 dependent friction law II: Dynamic friction. *Phys. Rev. B* **60**, 3928-3939 (1999).
- 213 19. Liu, Y. & Rice, J.R. Spontaneous and triggered aseismic deformation transients in  
214 a subduction fault model. *J. Geophys. Res.* **112**, B09404 (2007).
- 215 20. Ide, S., Beroza, G.C., Shelly, D.R. & Uchide, T. A scaling law for slow  
216 earthquakes. *Nature* **447**, 76-79 (2007).
- 217 21. Kostoglodov, V. et al. A large silent earthquake in the Guerrero seismic gap,  
218 Mexico. *Geophys. Res. Lett.* **30**, 1807 (2003).
- 219 22. Hirose, H., Hirahara, K., Kimata, F., Fujii, N. & Miyazaki, S. A slow thrust slip  
220 event following the two 1996 Hyuganada earthquakes beneath the Bungo  
221 Channel, southwest Japan. *Geophys. Res. Lett.* **21**, 3237-3240 (1999).
- 222 23. Hirose, H. & Obara, K. Repeating short- and long-term slow slip events with deep  
223 tremor activity around the Bungo channel region, southwest Japan. *Earth Plan.*  
224 *Space* **57**, 961-972 (2005).
- 225 24. Miyazaki, S., Segall, P., McGuire, J.J., Kato, T. & Hatanaka, Y. Spatial and  
226 temporal evolution of stress and slip rate during the 2000 Tokai slow earthquake.  
227 *J. Geophys. Res.* **111**, B03409 (2006).
- 228 25. Wallace, L.M. & Beavan, J. A large slow slip event on the central Hikurangi  
229 subduction interface beneath the Manawatu region, North Island, New Zealand.  
230 *Geophys. Res. Lett.* **33**, L11301 (2006).

- 231 26. Douglas, A., Beavan, J., Wallace, L. & Townend, J. Slow slip on the northern  
 232 Hikurangi subduction interface, New Zealand. *Geophys. Res. Lett.* **32**, L16305  
 233 (2005).
- 234 27. Ohta, Y., Freymuller, J.T., Hreinsdóttir, S. & Suito, H. A large slow slip event  
 235 and the depth of the seismogenic zone in the south central Alaska subduction  
 236 zone. *Earth Planet. Sci. Lett.* **247**, 108-116 (2006).
- 237 28. Rogers, G. & Dragert, H. Episodic tremor and slip on the Cascadia subduction  
 238 zone: The chatter of silent slip. *Science* **300**, 1942-1943 (2003).
- 239 29. Szeliga, W., Melbourne, T., Santillan, M. & Miller, M. GPS constraints on 34  
 240 slow slip events within the Cascadia subduction zone. *J. Geophys. Res.* **113**,  
 241 B04404 (2008).
- 242 30. Outerbridge, K.C. et al. A tremor and slip event on the Cocos-Caribbean  
 243 subduction zone as measured by a global positioning system (GPS) and seismic  
 244 network on the Nicoya Peninsula, Costa Rica. *J. Geophys. Res.* **115**, B10408  
 245 (2010).

246  
 247  
 248

### Figure Captions

249 **Figure 1: Overview of the Tohoku Region of the Japan Trench.** (Top Left) Map of the  
 250 Japan Trench area showing the locations of the JFAST drilling site C0019 (circle) and  
 251 seismic line HD33B (line within circle)<sup>13</sup>. Star indicates location of the  $M_w = 9.0$  Tohoku  
 252 earthquake. White bar indicates region of ~50 m coseismic slip from bathymetry data<sup>6</sup>.  
 253 Dashed box indicates area of the  $M_w = 7.0$  2011 SSE preceding the Tohoku earthquake<sup>9</sup>.

254 (Bottom) Seismic reflection profile for line HD33B<sup>13</sup>. (Top Right) Photo of a section  
 255 from Core 17R-1, the plate boundary fault zone. Scale at left in cm.

256 **Figure 2: Summary of Experimental Results.** (a) Example of shear stress and friction  
 257 data for an intact sample of the JFAST plate boundary fault zone (Core 17R-1). Boxes  
 258 and arrows indicate close-up views in following panels (b) Close-up view of friction data  
 259 showing the decrease from 10  $\mu\text{m/s}$  to 2.7  $\text{nm/s}$ .  $\Delta\mu_{ss}$  indicates the change in steady-state  
 260 friction used to calculate  $a-b$ . Box indicates the close-up view shown in panel c. (c)  
 261 Close-up view of stick-slip behavior, showing shear stress and displacement as a function  
 262 of time. Advances in displacement correlate with stress drops. (d) Close-up of 3-fold  
 263 increases in velocity. Inset shows a closeup view the 8.1 to 27  $\text{nm/s}$  velocity step data,  
 264 overlain by an inverse model from which the value  $a-b = 0.0034$  is obtained. (e) The first  
 265 slow instability in panel a, showing the shear stress (top), displacement of the sample  
 266 detrended for the remotely imposed slip velocity of 2.7  $\text{nm/s}$  (middle), and the time-  
 267 averaged instantaneous real slip velocity of the sample (bottom) as a function of time.  $\Delta\tau$   
 268 = stress drop. Detrended displacement set to 0 at the beginning of the event loadup phase,  
 269 decreasing values indicate slip deficit and positive values indicates slip accumulation.  
 270 Solid line on the velocity plot indicates prescribed driving velocity of 2.7  $\text{nm/s}$  for  
 271 comparison. (f) Same as panel e, for the second slow instability in panel a.

272 **Figure 3: Comparison of laboratory and natural SSE.** Slip velocity and duration of  
 273 laboratory SSE observed in JFAST samples compared with a selection of natural  
 274 subduction zone SSE<sup>2</sup> in Guerrero, Mexico<sup>21</sup>, the Bungo Channel (both short and long-  
 275 term SSE)<sup>22,23</sup> and eastern Nankai Trough (Tokai region) offshore Japan<sup>24</sup>, the Hikurangi  
 276 subduction zone offshore New Zealand near Manuwatu<sup>25</sup> and Gisborne<sup>26</sup>, southern

277 Alaska<sup>27</sup>, Cascadia<sup>28,29</sup>, and the Nicoya Peninsula, Costa Rica<sup>30</sup>. \*The total slip during  
278 our laboratory SSEs is probably limited by sample size, but using our laboratory-  
279 observed SSE slip velocities and assuming typically observed slip magnitudes of 2-20 cm  
280 results in event durations that match natural SSE.

281

## 282 **Methods**

283 We tested four samples in this study: two intact samples, and two powdered  
284 gouges. The intact samples were trimmed from whole-round cores parallel to the core  
285 axis, so that the fabric is aligned with the plane of shear. The powdered gouges were  
286 prepared by air drying fragments of the whole-round core, which were then crushed with  
287 a mortar and pestle to a grain size  $< 125 \mu\text{m}$ . The powders were then mixed with  
288 simulated seawater (3.5% NaCl brine) into a stiff paste and cold-pressed into the sample  
289 cell, which houses a cylindrical volume (25 mm diameter, 30 mm height). Both  
290 powdered and intact samples were tested with the sample cell flooded with seawater and  
291 thus tested in a fluid-saturated condition. The samples are confined by the sample cell  
292 and are not jacketed. All tests were performed at a constant temperature ( $\sim 20 \text{ }^\circ\text{C}$ ) in a  
293 climate-controlled room.

294 We conducted our experiments using a Giesa RS5 direct shear apparatus<sup>31</sup> (Supp.  
295 Figure 1). The sample cell is a stack of two steel plates which houses the cylindrical  
296 sample. Normal load is applied to the top face of the sample with a vertical ram, and held  
297 constant in servo-control via a proportional-integrative-derivative controller. We applied  
298 a normal stress of 7 MPa, comparable to in-situ effective stresses at the depth of sample  
299 recovery estimated from shipboard moisture and density measurements<sup>13</sup>. The sample

300 was then allowed to consolidate overnight (~18 hours) and is allowed to drain at the top  
301 and bottom faces via porous metal frits; the top is open to the atmosphere and the bottom  
302 to an open pore fluid reservoir within which the sample cell sits to prevent desiccation.  
303 Although we do not directly control the pore pressure, shearing was initiated after the  
304 compaction rate, measured as change in sample height over time, became negligible. We  
305 therefore assume that any excess pore pressure that may have developed during loading  
306 dissipates during the consolidation process and the applied stress equals the effective  
307 normal stress acting on the sample (pore pressure = 0). We further assume that because  
308 the sample maintains zero pore pressure during the experiment, the frictional behavior we  
309 observe is not attributable to fluctuations in said pressure.

310 The lower plate is displaced horizontally relative to the top plate by an electric  
311 motor, inducing planar (i.e. localized) shear deformation in the sample. The shear  
312 resisting force of the interface between the two plates is ~9 N, which we correct for in our  
313 measurements. For our samples, which have an area of  $5.07 \times 10^{-4} \text{ m}^2$ , the resolution of  
314 the load cells is 0.30 kPa in normal stress and 0.15 kPa in shear stress. Fluctuations due  
315 to electrical noise are estimated to be +/- ~0.4  $\mu\text{m}$  and +/- ~2 kPa. Displacement is  
316 measured directly at the sample cell by a potentiometric sensor with a resolution of 0.8  
317  $\mu\text{m}$ . Because the horizontal displacement sensor is located directly at the sample cell  
318 (rather than at the load cell) the recorded shear displacement represents the displacement  
319 of the sample without effects of apparatus stiffness. However, we also measure the  
320 apparatus stiffness by placing a separate displacement sensor at the horizontal load cell.  
321 Under a normal stress of 7 MPa, the horizontal stiffness is 3.8 kN/mm. The stiffness of  
322 the apparatus was not modified for these experiments. The displacement record at the

323 sample cell is a measured value, which is distinct from the driving velocity enforced by  
 324 the motor near the load cell. We utilize a stepper motor with an update rate of 0.19 Hz  
 325 and a step width of 0.015  $\mu\text{m}$ , and recorded our data at 0.033 Hz (or 10 measurements  
 326 every 0.81  $\mu\text{m}$  defined by the displacement sensor resolution) for a time-averaged  
 327 displacement rate of 2.7 nm/s.

328 We measure the shear strength  $\tau$  throughout the experiment, which we use to  
 329 calculate an apparent friction coefficient  $\mu$ :

$$330 \quad \mu = \frac{\tau}{\sigma_n}, \quad (1)$$

331 Assuming (1) that the cohesion is negligible, and (2) that any pore pressure fluctuations  
 332 are small so that the applied normal stress equals the effective normal stress throughout  
 333 the experiment.

334 We measure the velocity-dependence of friction as:

$$335 \quad a - b = \frac{\Delta\mu_{ss}}{\Delta \ln V} \quad (2)$$

336 where  $\Delta\mu_{ss}$  is the difference in steady-state friction before and after a change in slip  
 337 velocity  $V$ . Determination of steady-state is an approximation by which no obvious slip-  
 338 hardening or weakening trends are present where the measurement is made. For the  
 339 decrease in slip velocity from the background rate of 10  $\mu\text{m/s}$  to the plate-rate of 2.7  
 340 nm/s, we calculate  $a-b$  by directly measuring  $\Delta\mu_{ss}$ . We also conducted velocity-stepping  
 341 tests using three-fold (half-order of magnitude) increases in slip velocity at 2.7, 8.1, 27,  
 342 and 81 nm/s. The frictional response to a velocity step is described by the RSF relations:

$$343 \quad \mu = \mu_o + a \ln\left(\frac{V}{V_o}\right) + b_1 \ln\left(\frac{V_o \theta_1}{D_{c1}}\right) + b_2 \ln\left(\frac{V_o \theta_2}{D_{c2}}\right) \quad (2)$$

344 
$$\frac{d\theta_i}{dt} = 1 - \frac{V\theta_i}{D_{c_i}}, i = 1, 2 \quad (3)$$

345 Where  $a$ ,  $b_1$  and  $b_2$  are dimensionless constants,  $\theta_1$  and  $\theta_2$  are state variables (units of  
 346 time), and  $D_{c1}$  and  $D_{c2}$  are critical slip distances over which friction evolves to a new  
 347 steady state value<sup>32</sup>. If the data are well described by a single state variable then  $D_{c1} =$   
 348  $D_{c2}$  and we take  $b_2 = 0$ ; to account for the possibility of one or two state variables we  
 349 define  $b = b_1 + b_2$ . Equation 3 describes the evolution of the state variable  $\theta$  and is  
 350 known as the “Dieterich” or “slowness” law, which has the property that friction can  
 351 change as a function of time even in the limiting case of zero slip velocity<sup>32</sup>. The  
 352 individual RSF parameters  $a$ ,  $b_1$ ,  $b_2$ ,  $D_{c1}$  and  $D_{c2}$  must be determined by inverse modeling  
 353 using an iterative least-squares method that also accounts for elastic interaction with the  
 354 testing machine<sup>33,34</sup>. This requires an expression for the system stiffness  $k$   
 355 (friction/displacement):

356 
$$\frac{d\mu}{dt} = k(V_{lp} - V). \quad (5)$$

357 Conventionally,  $(V_{lp}-V)$  is defined as the difference between true fault slip velocity  $V$  and  
 358 the remotely recorded load point velocity  $V_{lp}$ , and  $k$  is the stiffness of the testing machine,  
 359 which includes the forcing blocks and support structure, and the fault zone of finite  
 360 width. For our apparatus stiffness (3.8 kN/mm) and sample dimensions ( $5 \times 10^{-4}$  m<sup>2</sup>) this  
 361 results in  $k = \sim 1$  mm<sup>-1</sup>. Our modeling procedure also allows the removal of long-term  
 362 slip-dependent friction trends, in order to avoid biasing and more accurately determine  
 363 the friction velocity dependence<sup>34</sup>. Although the modeling technique is a more robust  
 364 method of determining  $a-b$ , it is difficult to apply to large, negative velocity differences



365 and therefore was not used for the decrease from the background velocity to plate  
366 convergence velocity.

367

368 **Methods References:**

369 31. Ikari, M.J., Hüpers, A., & Kopf, A.J. Shear strength of sediments approaching  
370 subduction in the Nankai Trough, Japan as constraints on forearc mechanics.

371 *Geochem. Geophys. Geosyst.* **14**, 2716-2730 (2013).

372 32. Dieterich, J.H. in *Mechanical Behavior of Crustal Rocks* Vol. 24 (eds. Carter, N.L. et  
373 al.) 102-120 (Geophys. Monogr, Ser., 1981).

374 33. Reinen, L.A. & Weeks, J.D. Determination of rock friction constitutive parameters  
375 using an iterative least squares inversion method. *J. Geophys. Res.* **98**, 15,937-

376 15,950 (1993).

377 34. Blanpied, M.L., Marone, C.J., Lockner, D.A., Byerlee, J.D. & King, D.P.

378 Quantitative measure of the variation in fault rheology due to fluid-rock  
379 interactions. *J. Geophys. Res.* **103**, 9691-9712 (1998).

380

381 **Supplementary Figure 1:** Schematic diagram of the single-direct shear apparatus. Not  
382 to scale.

383 **Supplementary Figure 2:** Coefficient of friction as a function of shear displacement for

384 tests on intact JFAST fault zone samples in this study. Velocity steps were

385 performed in experiment B384, which is also shown in main text Figure 2.

386 **Supplementary Figure 3:** Coefficient of friction as a function of shear displacement for

387 tests on powdered JFAST fault zone samples in this study. Velocity steps were

388 performed in experiment B525. Significant slip weakening at the end of the tests  
389 with powdered samples is attributed to sample extrusion from the testing cell.  
390 Note that SSE occur far less frequently in powdered samples.

391 **Supplementary Figure 4:** Coefficient of friction as a function of shear displacement for  
392 samples of Rochester shale as a control experiment for comparison (B524),  
393 prepared in an identical manner to the JFAST samples. Of note: (1) no SSE-type  
394 shear stress excursions occur at 2.7 nm/s for this material, (2) no stick-slip occurs  
395 in this material, (3) friction decreases following the decrease in slip velocity,  
396 signifying velocity-strengthening friction, and (4) velocity-steps (positive  
397 increases in velocity) also indicate velocity-strengthening friction.

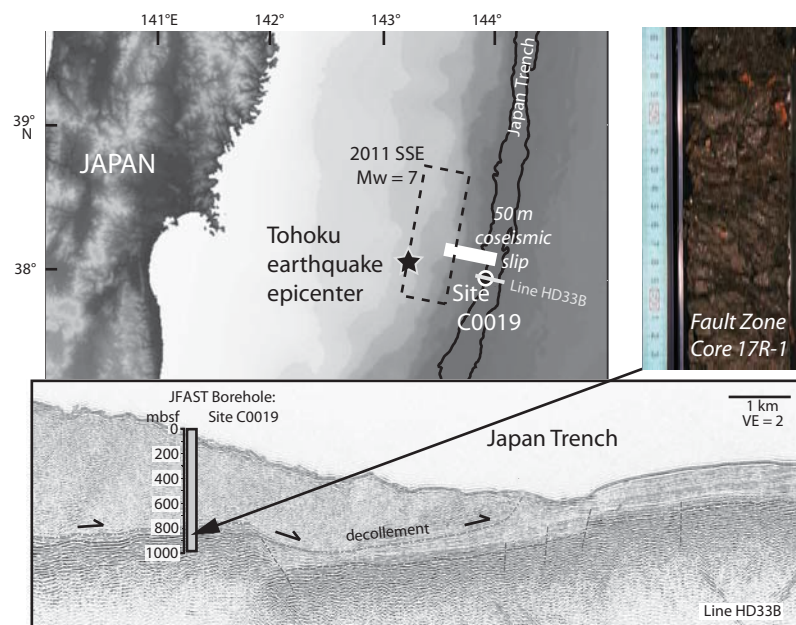


Figure 1: Ikari et al., Japan Trench Instability

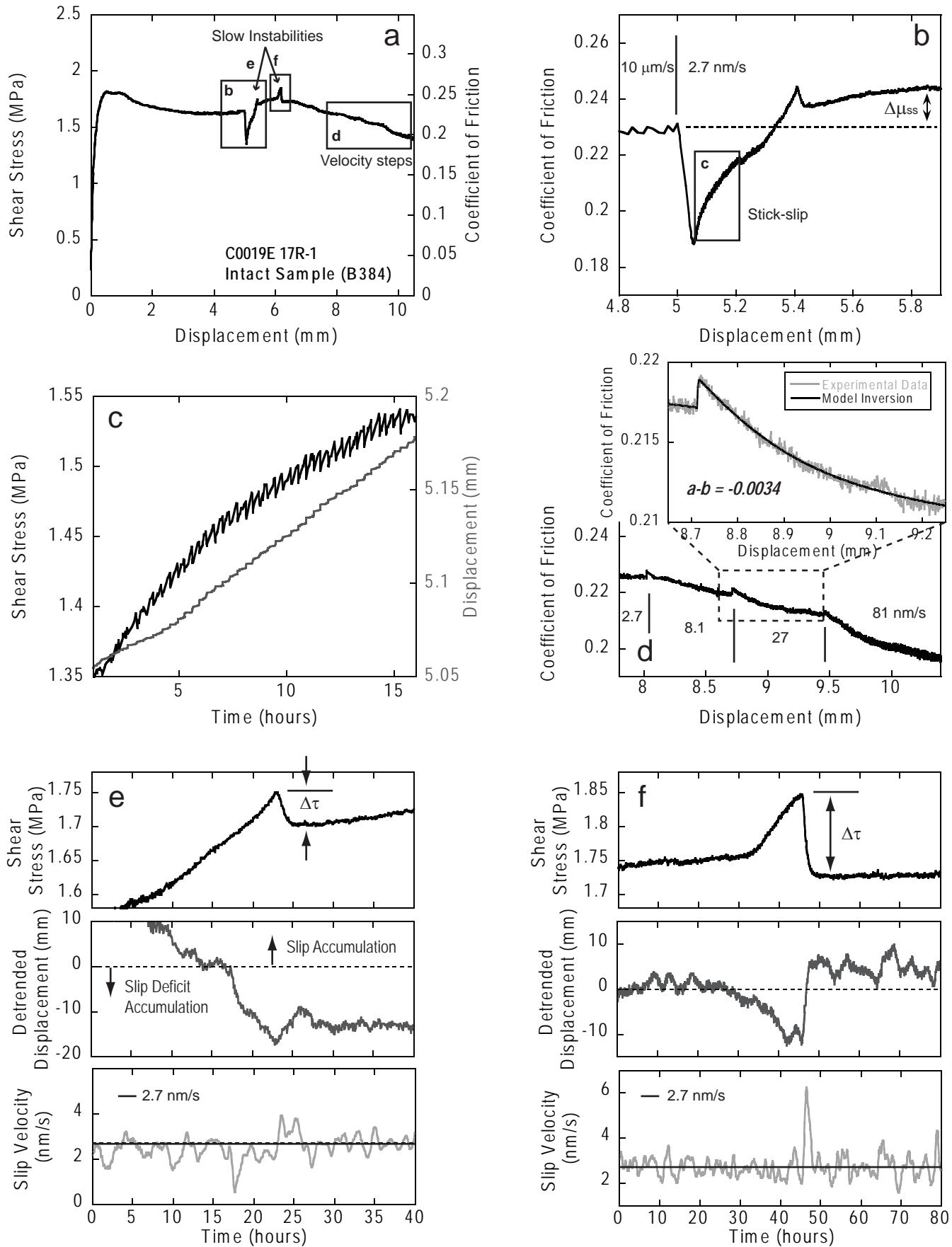


Figure 2: Ikari et al., Japan Trench Instability

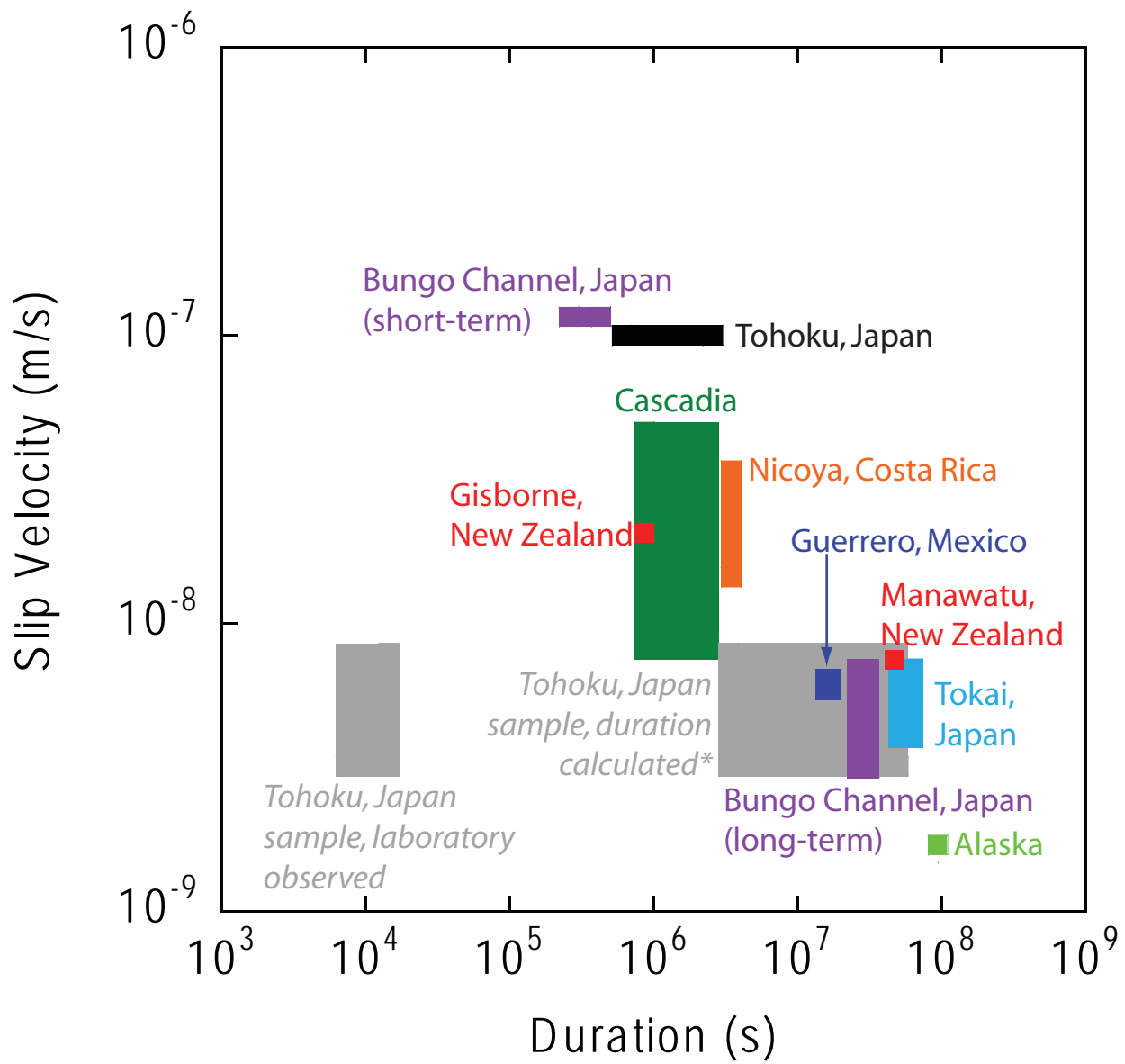


Figure 3: Ikari et al., Japan Trench Instability